Tracking of melanoma cell plasticity by transcriptional reporters

Anna Vidal[1,2] and Torben Redmer[1,2,3]*

1   University of Veterinary Medicine, Vienna, Austria
2   Institute of Medical Biochemistry
3   Institute of Pathology, Unit of Laboratory Animal Pathology

Contact: Anna.Vidal@vetmeduni.ac.at, Torben.Redmer@vetmeduni.ac.at

*   Correspondence: Torben.Redmer@vetmeduni.ac.at; Tel.: +43 1 250-77-2423

Abstract: Clonal evolution and cellular plasticity are the genetic and non-genetic driving forces of tumor heterogeneity that in turn determines the tumor cell response towards therapeutic drugs. Several lines of evidence suggest that therapeutic interventions foster the selection of drug resistant neural crest stem-like cells (NCSCs) that establish minimal residual disease (MRD) in melanoma. Here we established a dual reporter system enabling the tracking of NGFR expression and mRNA stability, providing insights into the maintenance of NCSC-states. We observed that the transcriptional reporter that contained a 1kb fragment of the human NGFR promoter was activated only in a minor subset (0.72±0.49%, range 0.3-1.5) and ~2-4% of A375 melanoma cells revealed stable NGFR mRNA. The combination of both reporters provided insights into phenotype switching and revealed that both cellular subsets gave rise to cellular heterogeneity. Moreover, whole transcriptome profiling and gene set enrichment analysis (GSEA) of the minor cellular subset revealed hypoxia-associated programs that might serve as potential drivers of an *in vitro* switching of NGFR-associated phenotypes and relapse of post-BRAF inhibitor treated tumors. Concordantly, we observed that the minor cellular subset increased in response to dabrafenib over time. In summary, our reporter-based approach provided insights into plasticity and identified a cellular subset that might be responsible for the establishment of MRD in melanoma.

Keywords: Transcriptional reporters; Plasticity; Stemness; NGFR

1. Introduction

The emergence of therapy-resistant tumor cell clones is frequently observed in melanoma patients and responsible for tumor relapse and poor prognosis. Recently a neural crest-stem cell (NCSC)-like signature has been identified determining minimal residual disease in melanoma[1]. Hence, high levels of NCSC genes likely confer intrinsic resistance to inhibition of BRAF and MEK, among them NGFR. The expression of the latter nerve growth factor receptor (CD271) and putative marker of melanoma initiating cells sufficiently mediated resistance to vemurafenib *in vitro* and was associated with lymph node metastasis in melanoma patients[2-7]. Melanoma cells expressing NGFR exhibit increased migratory, invasive and survival capacities and the knockdown of this TNF-receptor family member revealed a network of NGFR/CD271-associated genes that facilitate and maintain the different phenotypes[8-12]. Although NGFR-mediated signaling mechanisms are still not well understood in melanoma and cancer, several lines of evidence suggest that NGFR serves as a regulator of basic tumor cell properties such as plasticity, hence non-genetic and reversible switching of cellular phenotypes[13-16], likely triggered by environmental cues causing stress. Concordantly, NGFR was highly expressed in chemoresistant melanoma cells[10].

Here we established a dual-reporter system that enabled the tracking of NGFR expression over time and demonstrated the phenotype switching capacity of isolated cellular subsets in response to therapeutic drugs.

2. Results and Discussion

A dual NGFR-reporter revealed phenotype switching of melanoma cells

Melanoma cells feature a high capacity of cellular plasticity, a non-genetic process that likely enables the adaptation to environmental cues such as changes in growth factor conditions or the interaction with extracellular matrix components[33]. In addition, cellular plasticity probably controls the interconversion of stem-like and non-stem-like tumor cells. The expression of NGFR/CD271 was associated with melanoma cell stemness[3,11,12,23], however we observed that the CD271+ population contains a label-retaining subset and hence comprises a proliferating non-stem like and a slow-cycling fraction that likely presents the actual subset of melanoma initiating cells[11,12]. These previous findings suggest that CD271 labels a heterogeneous pool of melanoma cells which likely feature unique and common properties. We established a double-reporter system that combines the transcriptional activation of a 1kb fragment of the NGFR promoter that controls expression of RFP and of a sequence of the 3′-UTR of NGFR that controls the stability of GFP, expressed under control of a cytomegalovirus (CMV) promoter. The NGFR promoter sequence comprised a region of 900 bp upstream to 100 bp downstream from the transcriptional start site (Figure S1A) and contains binding sites for early growth response protein 1 (EGR1). The latter in turn has been associated with control of NGFR expression[35]. Hence, the reporters reflected two states of NGFR expression, the transcriptional activation of the NGFR promoter and the regulation of mRNA stability (Figure 1A, left schemes). The sequential lentiviral transduction of A375 cells revealed the co-existence of four discrete cell states, GFP+/RFPneg, GFP+/RFP+, RFP+/GFPneg and GFPneg/RFPneg (Figure 1B, right panel). Next, we asked whether the different cell states that were investigated ~14d post infections and selection for puromycine resistance presented stable or interconvertible states, hence reflected phenotype switching. To this end, we analyzed the levels of GFP and RFP 7d after a FACS-based isolation of subsets presenting the four cell states and hypothesized that the double positive subset constituted an intermediate state. We investigated the occurrence of GFP+, RFP+, double positive and negative subsets and observed that all four cell states emerged from the different isolated subsets (Figure 1B, C). Moreover, we observed that GFP+ cells showed a lower cell surface expression of CD271 than RFP+ cells, suggesting that the transcriptional reporter superiorly reflected the levels of CD271 and the expression of GFP indeed recapitulated the post-transcriptional regulation. Although FACS-based enrichment was highly efficient, we could not fully exclude that subsets might contained admixed cells of other subsets. Therefore, we investigated the emergence of different cell states from double negative and positive subsets. We observed that all four cell states emerged from double negative cells over time (Figure S1B) and maintained expression of the melanoma marker KBA.62. In addition, we observed that even double positive cells were capable of developing double negative cells (Figure 1C, lower row). Likely, double positive cells presented an intermediate population that featured a multipotent, stem-like capacity. However, intrinsic programs might control the capacity of renewing the NGFR+ cell pool independent from the initial phenotypes. Therefore the reporters recapitulated the plasticity of NGFR/CD271+ phenotypes of *in vitro* cultured cells as reported in previous studies[24,25]. However, the *in vivo* stability and sustainability of the NGFR/CD271+ phenotype of melanoma cells is unknown and possibly inaccessible for investigation.

We validated the functionality of the transcriptional reporter in A2058 cells (Figure S1C); however, we observed a high reliability of the transcriptional reporter only in A375 cells. Generally, we observed a high concordance of reporter activation and cell surface levels of CD271 but also found minor subsets that featured activation of the transcriptional reporter (RFP+) but showing only a low level of CD271 (Figure 1D, left panels). This discrepancy might reflect different regulatory circuits controlling the level of CD271 expression. In summary, the NGFR double reporter system enabled the tracking of phenotype switching and demonstrated the multipotent capacity of melanoma cells (Figure

1D, right panel) although low-passage, patient-derived melanoma cells might feature a different turnover of cellular phenotypes.

Whole transcriptome profiling revealed a hypoxic phenotype of cellular subsets

RFP^{+} cells sufficiently renewed the stem-like cell pool by symmetric cell division (Figure 2A) and gave rise to all subsets. Therefore we asked next for the molecular programs activated in the minor cellular subset that featured activation of the transcriptional reporter. We determined the proportion of proliferative/Ki67^{+} cells within the RFP[+] subset and observed that a high proportion of RFP[+]/Ki67^{+} cells by flow cytometry (89.6%) and quantitative immunofluorescence microscopy (54.2±7.6%), (Figure 2B). Next, we performed a whole transcriptome profiling of FACS-isolated RFP[+] and unsorted bulk cells and identified 607 differentially regulated genes (p<0.001) among them the ABC transporter ABCC2, MMP1 (matrix metalloproteinase 1), IL24 (interleukin 24) and the hypoxia induced TXNIP (thioredoxin interacting protein), (Figure 2C, left panel). Concordantly, gene-set enrichment analysis (GSEA) revealed a significant enrichment of signature genes of hypoxia, EMT (epithelial-to-mesenchymal transition) and TNFα-induced NFκB signaling (Figure 2C, right panel). In addition, we performed a single-sample GSEA and observed the separation of RFP[+] and bulk cells by signatures that are associated with hypoxia, stemness and NFκB signaling (Figure 2D). The expression of CD271 is linked to neural-crest cell stemness in melanoma and the downregulation of NGFR/CD271 abrogated all features of a neural crest stem cell (NCSC)-like state[11]. We asked whether RFP^{+} cells featured a NCSC-like or intermediate cell state. Indeed, GSEA revealed a proliferative and transitory-melanocytic rather than a NCSC state (Figure 2E). This finding underpinned the heterogeneity of the CD271^{+} cell pool that comprised proliferating and likely non-proliferating cells. However, we observed that only a very rare subset of cells indeed exhibited a slow-cycling phenotype and the majority of cells lost the labeling by the lipophilic dye PKH67 over time. In addition, the label-retaining capacity of the RFP[+] subset and bulk cells was comparable (Figure S1D).

NGFR/RFP^{+} cells are enriched upon dabrafenib treatment reflecting a MAPKi-driven hypoxic-phenotype

Several lines of evidence suggest a therapy-driven enrichment of intrinsically resistant stem-like melanoma cells establishing minimal residual disease (MRD) a driving force of relapse in melanoma patients. We investigated pre- and post-treatment melanoma specimens of patients who received a BRAFi/MEKi (dabrafenib/trametinib) therapy and developed therapy-resistant progressive disease (GSE7794027). The expression of NGFR but not of ABCB5 an additional marker of melanoma stem-like cells[34] was increased in five of six post-treatment tumors (p=0.004; two-sided paired t-test) and was accompanied by decreased levels of E-cadherin/CDH1 (Figure 3A, left panel). Moreover, GSEA revealed an enrichment of hypoxia-related genes, hence suggesting the activation of a hypoxia-related program in relapsed tumors (Figure 3A, right panel).

We asked whether the minor cellular subset as marked by activity of the transcriptional reporter presented an MRD-establishing cell clone. As we expected that the clone featured resistance towards dabrafenib we performed a live cell imaging-based tracking of A375[CD271-RFP] reporter cells for 72-96h and analyzed changes in the proportion of RFP^{+} cells over time. Reporter cells showed a general response towards dabrafenib in a range of 1-3nM (IC50=2.148nM) and a dose-depending increase in the number of RFP^{+} cells (Figure 3B and S2A-B) in a range according to IC50. The dabrafenib response of reporter cells was evident even 48h after treatment and reached a maximum after 72-92h (Figure 3C and S2B) and was not accompanied by changes in the number of GFP^{+} cells (data not shown). However, this increase very likely reflected the dabrafenib-induced activation of the reporter and potentially marked melanoma cells that featured MRD. Next, we assessed whether gene signatures mirroring a *in vivo* drug response and potentially reflected MRD-states were enriched in the RFP[+] minor subset. Although we observed a

partial enrichment of signatures by GSEA, none of the MRD-associated gene signatures showed a significant enrichment in the RFP⁺ subset (data not shown).
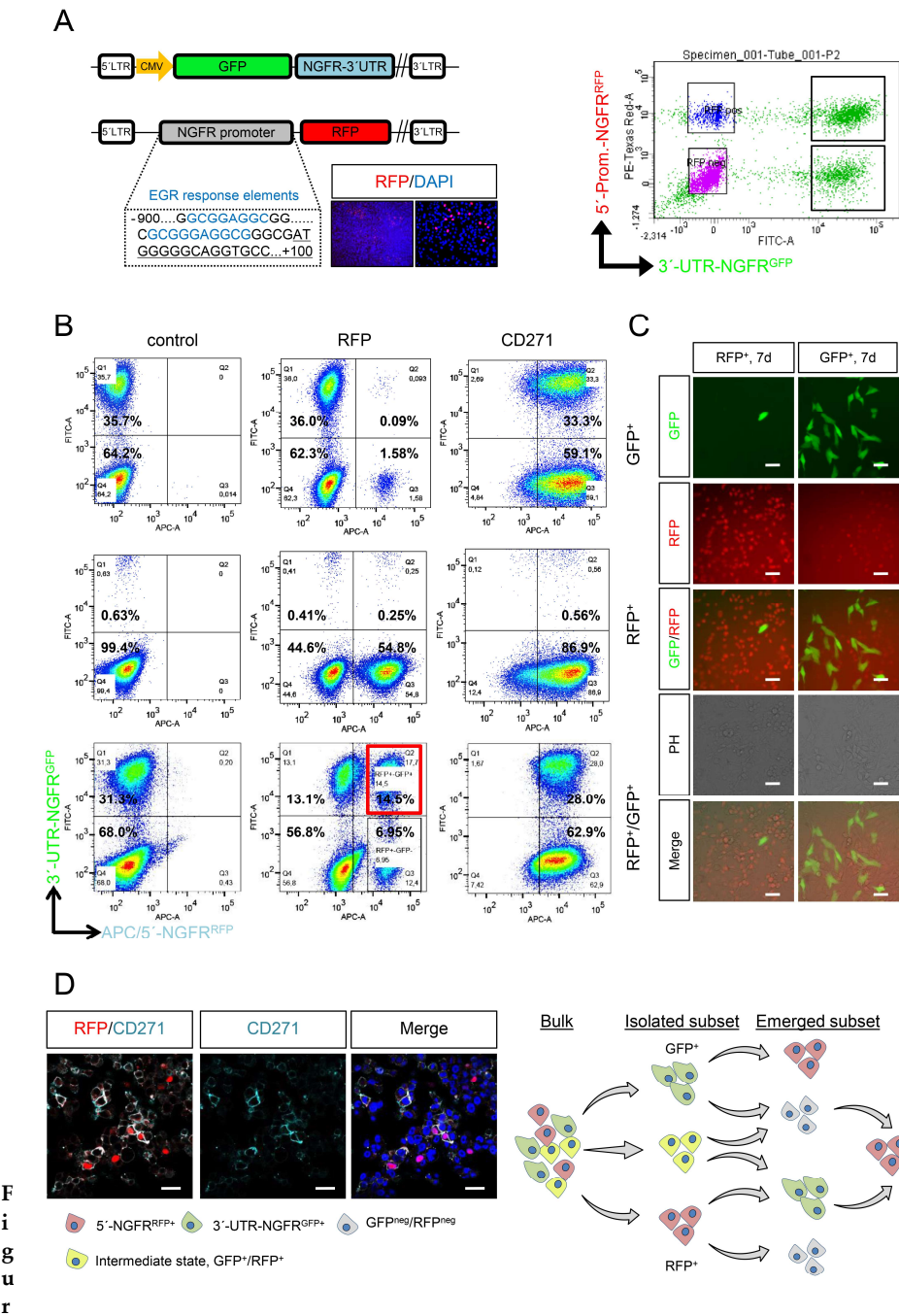
Figure 1. A dual-reporter system enabled tracking of phenotype switching. A.) Simplified plasmid maps of 3′-UTR-NGFR miRNA reporter that expressed GFP fused to 3′-UTR of the NGFR gene under control of a CMV promoter (upper map) and of a customized NGFR reporter that expressed RFP under control of a 1kb fragment of the NGFR promoter that contained EGR response elements (lower map). Images depict indirect detection of RFP⁺ cells using an RFP-specific antibody. A FACS

plot indicates the presence of four distinct cellular subsets regarding the expression of reporters that were stably expressed in A375 cells (right panel). B.) Flow cytometric analysis of FACS-isolated cellular subsets GFP[+], RFP[+] or (double positive (GFP[+]/RFP[+]) 7d post isolation for levels of GFP, RFP and cell surface expression of CD271; 50,000-100,000 cells were recorded. C.) Immunofluorescence microscopy of A375 reporter cells analyzed in (B) showing the distribution of cellular subsets. Bars indicate 50 µm. D.) Confocal microscopy of reporter cells stained for RFP and CD271 indicating distinct and co-occurrence of both. Bars indicate 50 µm, DAPI served as nuclear stain (left panels). Schematic representation of phenotype switching processes as tracked by the dual-reporter system.

As hypoxia serves as a driving force of therapy resistance[26], we asked whether the hypoxic phenotype of RFP^{+} cells might aid cells escaping from a dabrafenib-mediated downregulation of proliferative programs. We observed that the hypoxia inducible transcription factors EGR1 and ATF3 are significantly higher expressed in RFP[+] than bulk cells (Figure 3D, left panel, Table S1) and likely mediated the reporter activation in response to dabrafenib by binding to their respective sites in the NGFR promoter. Hence, the hypoxia driven expression of both transcription factors might be responsible for the increased expression of CD271/NGFR in response to dabrafenib.

**Fi
gu**
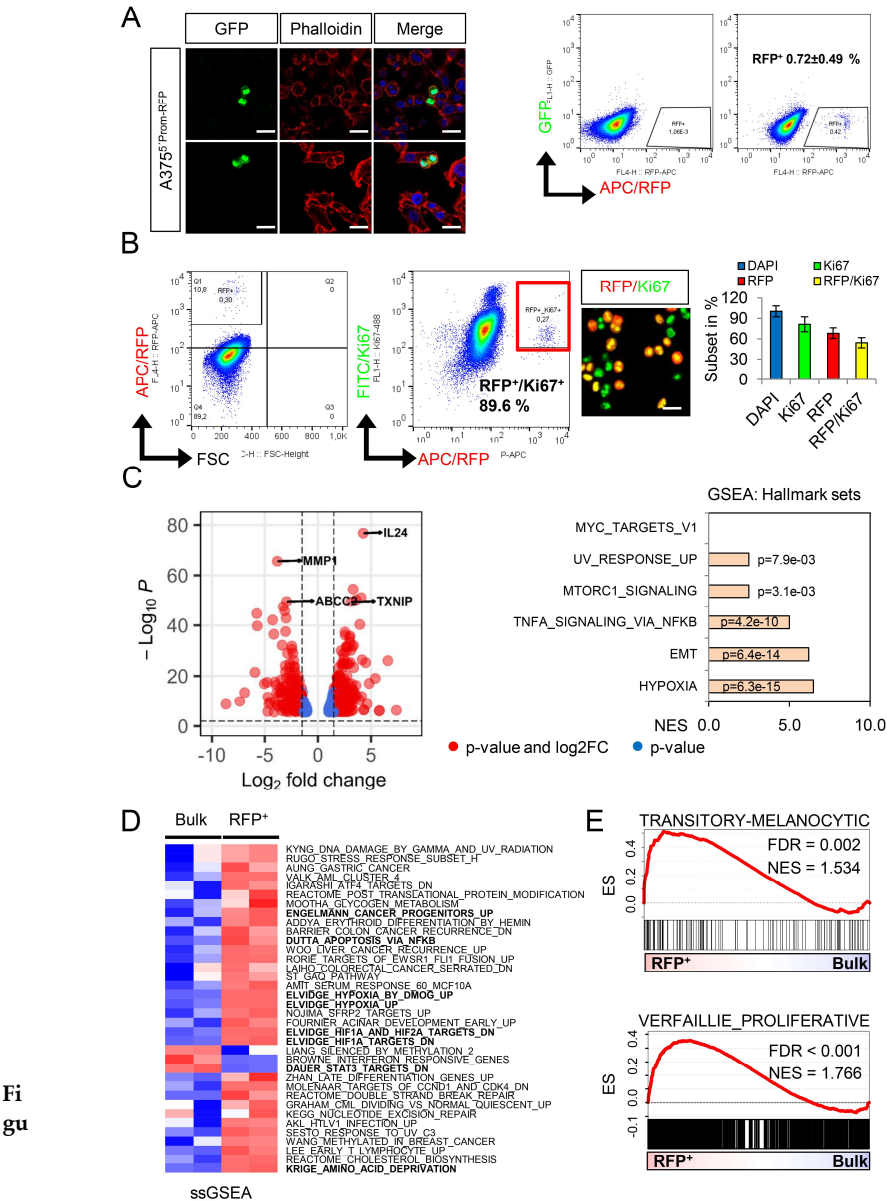
re 2. A minor cellular subset featured a hypoxic and proliferating phenotype. A.) Confocal microscopy of reporter cells revealed a symmetric division of RFP⁺ cells (left panels) and flow cytometry indicates the low abundance of A375 cells showing activation of the transcriptional reporter. 10,000 cells were recorded. B.) A flow cytometric analysis of RFP⁺ cells revealed a high percentage of proliferating, Ki67⁺ cells within the RFP⁺ cell pool (left panels), increased in RFP⁺ enriched cells (right panels). C.) Volcano plot depicts the top differentially regulated genes (DEGs, p<0.001) as identified by whole transcriptome profiling of RFP⁺ cells showing that IL24 and TXNIP or MMP1 and ABCC2 were among the top up or down regulated genes, respectively (left panel). GSEA of DEGs revealed enriched Hallmark signatures with Hypoxia and EMT as most significantly enriched pathways in RFP⁺ cells (right panel). Single-sample GSEA revealed that hypoxia-associated gene signature, among others significantly (p<0.001) separated RFP⁺ from bulk cells. E.) Enrichment plots indicate the predominance of genes that are associated with a transitory-melanocytes or proliferative cell phenotype.
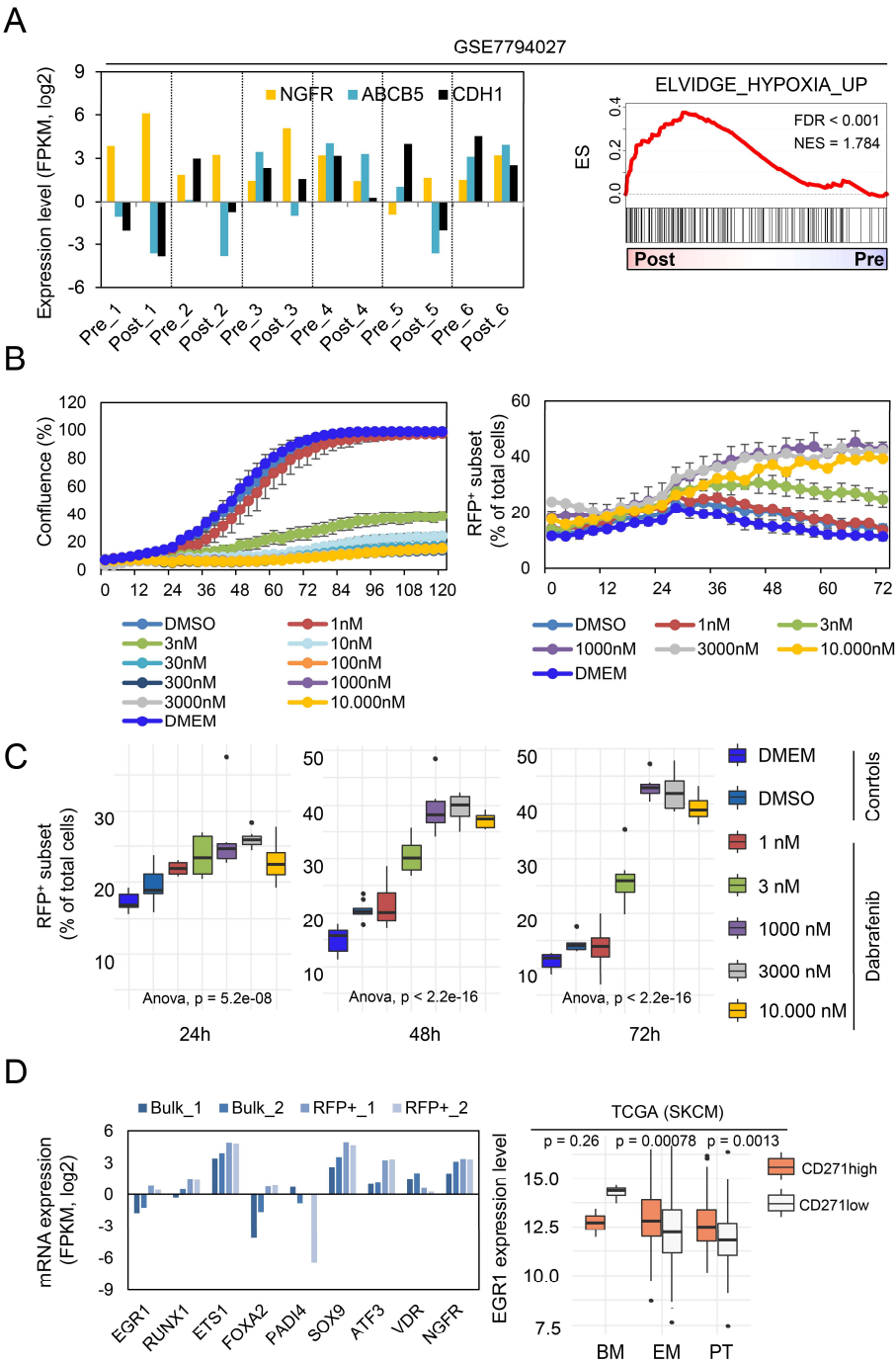
Figure 3. Dabrafenib treatment increased the emergence of resistant cell clones. A.) FPKM (log2) expression levels of markers of a melanoma stem-like state NGFR and ABCB5 and the epithelial marker E-cadherin (CDH1) in six pre-BRAFi treatment and post-relapse patient-derived tumors of melanoma origin (GSE7794027), (left panel). GSEA of public data analyzed in (A) for enrichment of hypoxia-associated genes shows enrichment of hypoxia-related genes in the group of therapy-resistant, relapsed tumors (right panel). ES=enrichment score; NES=normalized enrichment score B.) Live cell-imaging based dose-response of reporter cells towards dabrafenib. Drug response is indicated by changes in confluence (%), left panel. Increase in the number of RFP⁺ cells as depicted in % of total cells of dabrafenib treated cells (right panel). Values are shown as mean±sdv of eight technical replicates, a representative out of three experiments is shown C.) Box plot representation of cell density at 24, 48 and 72 hours after treatment depict a significant difference in the number of RFP⁺ cells, depicted as % of total cells (right panel). D.) Expression levels of top differentially regulated genes among RFP⁺ and bulk cells, log2 FPKM values of two independent biological replicates are shown (left panel). Box plot representation of levels of EGR1 expression in the set of TCGA melanoma (PT, primary melanoma; EM, extracranial and BM, brain metastases) ranked by expression of CD271/NGFR, significance was determined by a two-way anova.

Indeed, ATF3 and NGFR were top enriched in vemurafenib-treated COLO858 cells[28], and EGR1 expression was significantly increased in the CD271/NGFR^high subset of melanoma (TCGA data) (Figure 3D, right panel). The binding of EGR1 to the NGFR promoter was previously shown[35], suggesting that EGR1 might act in concert with ATF3 and tightly controlled the expression of CD271 during phenotype switching. Finally, we investigated the potential regulation of general markers of melanoma (PD-L1, MET) and of additional mediators of stemness and phenotype switching besides NGFR such as SOX9, ATF3 and TMEM47[36-42] in RFP positive (RFP) or negative (-) sorted cells four and eight days after sorting. We observed increased expression levels from day four to eight, particular ATF3 and NGFR revealed a steady increase in expression levels (Figure S2C). Therefore, additional markers are likely regulated by phenotype switch. Particularly, the regulation of PD-L1 the target of immune checkpoint inhibitor-based therapies may determine the efficacy of therapeutic interventions targeting a certain cell surface molecule[43].

In summary, we established here a NGFR reporter system that enabled the tracking of phenotype switching and drug response and uncovered a potential role of hypoxia and hypoxia-induced gene expression for the emergence progressive dabrafenib-resistant melanoma.

3. Materials and Methods

Cell culture

A375 and A2058 (purchased from ATCC) were kept at 37 °C, 5% CO2 and 95% humidity in cell culture medium (DMEM, 4.5 g/L glucose, stabilized glutamine/GlutaMax, pyruvate) supplemented with 10% fetal bovine (Gibco/Thermo fisher) serum and 1% penicillin/streptomycin (Gibco/Thermo fisher) as previously reported[11]. Cells were seeded onto 8-chamber glass slides to a density of 5,000-10,000 cells per chamber for imaging. Label-retention assays were performed as previously described[11].

Flow cytometry/Fluorescence-activated cell sorting (FACS)

After removal of medium, cells were washed with 1X phosphate buffered saline (PBS) and harvested by trypsin (0.05 % trypsin/EDTA). Following addition of cell culture medium, cells were collected by centrifugation at 1,000 rpm at room temperature for 3 minutes (min) and resuspended in 100 µl of ice cold buffer (1X PBS/0.5 % bovine serum/2 mM EDTA) and stored on ice. Cells were incubated with primary antibodies CD271-APC (Miltenyi), RFP (NovusBiologicals) or KBA.62 (BioLegend) all diluted to 1:80 in buffer and stored at 4°C for 10 min to achieve proper labeling. Following, cells were washed with buffer and incubated with secondary antibodies (AlexaFluor-488/594/647, diluted to

1:500) and incubated as mentioned above. Washed cells were resuspended in 500 μl PBS and analyzed by flow cytometry (Canto II). The isolation of reporter cells was performed with AriaIII (Becton&Dickinson) regarding their levels of GFP and RFP, collected in cell culture medium and expanded under normal cell culture conditions. Data analysis was performed with FlowJo (Ver 10.7.1). FACS-isolated cells were collected in cell culture medium and seeded on appropriate vessels following centrifugation.

Production of lentiviral particles

Briefly, for production of lentiviral particles, LentiX cells were seeded to 1×10^4 cells on a 10 cm dish and transfected after 24h with 4 μg of a plasmid expressing GFP fused to the 3´-untranslated region (UTR) of NGFR (abmgood, #3180008) to elucidate the interactions between miRNAs and the 3'UTR of the NGFR gene or a customized plasmid that contained a 1kb promoter (-900; +100) of the human NGFR gene and the coding sequence of red fluorescent protein (RFP). The RFP reporter plasmid was customized by Applied Biological Materials Inc. (abm). For generation of viral particles, LentiX cells were transfected with 2 μg of pMD2.G (addgene # 12259, VSV-G envelope) and 1 μg of psPAX2 (#12260) packaging plasmids using 20 μl/1ml PEI (Polyethylenimine, Sigma-Aldrich). Medium was changed after 24h and viral supernatant was harvested after additional 24h. Viral supernatants were filtered through a 0.45 μm filter and applied to target cells for 24-48h. Infected cells were selected for resistance to puromycin (10 μg/ml).

Live cell imaging-based drug assays

The response of A375 cells to dabrafenib in a range of 1nM-10μM of eight technical replicates was assessed by live-cell imaging-based drug responses using the IncucyteS3 live cell imaging microscope (EssenBioscience/Sartorius) 24h after seeding of 2,500 cells/100 μl/96-well and addition of serially diluted compounds. Images were take every three hours using a 10x objective and the general label-free mode, two pictures of eight technical replicates per condition were taken. Drug response was assessed by changes in the cellular density over time. The cell density was determined by a confluence mask tool of as part of the Incucyte software. IC50 values were calculated by curve-fitting (https://search.r-project.org/CRAN/refmans/ REAT/html/curvefit.html) based on confluence measurements at day 3 and Incucyte software tools.

Immunofluorescence and confocal microscopy

Briefly, following removal of medium cell grown in chamber slides were washed once with PBS and fixed with PFA (paraformaldehyde, 4% in PBS) for 10 min at room temperature. After fixation, washed cells were incubated with primary antibodies p75NTR (Cell signaling, 1:100) and RFP (NovusBiologicals, 1:200) were diluted in blocking buffer PBS, 2% fetal serum albumin) overnight at 4°C. Next day, cells were washed and incubated with secondary antibodies (AlexaFluor-488/594/647, diluted to 1:500) and DAPI (4',6-Diamidino-2-phenylindole, diluted to 1:500) and incubated for 1h at room temperature, protected from light. Following, slides were covered with mounting medium and cover slips and store at 4°C until imaging.

High-resolution immunofluorescent imaging of tumor sections and cell lines was performed with LSM880 airyscan confocal microscope (Zeiss) and appropriate software (Zen black, ver. 2.3 SP1). Images were taken with objectives 10x, 20x and 63x/1.40 plan-apochromat, oil dic M27) at a resolution of 2048x2048 pixels/cm, 8bit, scan speed 6, averaging 4. Imersol 518F was used for oil microscopy. Stacked multichannel image files (czi) were separated and background adjusted using AdobePhotoshop2020 and stored as merged tiff files at a resolution of 600 dpi.

RNA isolation and sequencing

Briefly, isolation of total RNA of snap frozen or intraoperative tumors was performed with the RNAeasy extraction kit (Quiagen) according to the manufacturer's instructions. RNA integrity was determined by automated electrophoresis (4200 TapeStation system, Agilent). The library preparation of 100 ng total RNA was performed with TruSeq Stranded total RNA Sample Preparation-Kit and Ribo Zero Gold (Illumina) and paired-end (2x100 bp) whole transcriptome profiling of RNA with integrity numbers (RIN) ≥7 was performed at Cegat GmbH, Tuebingen (Germany) and sequenced on NovaSeq6000 platform. Illumina bcl2fastq (2.19) was used for a demultiplexing of sequenced reads and adapter trimming was performed with Skewer (version 0.2.2)[17]. The information on FASTQ files was obtained using the FastQC program (version 0.11.5-cegat) read out. Raw sequencing data (fastq files) were quality controlled using fastqc (version 0.11.7 - Bioinformatics Group at the Babraham Institute) and further preprocessed with fastp[18]. Reads were aligned to the GRCh38 version of the human genome using TopHat19 and counts per gene were calculated by the featureCount-algorithm from the Rsubread package[20]. All further steps of the analysis were done in R. Raw counts of protein-coding genes were normalized using the DESeq2 (https://bioconductor.org/packages/release/bioc/html/DESeq2.html) package[21]. Differential expression of genes between groups was determined after fitting models of negative binomial distributions to the raw counts. Raw p-values were fdr-adjusted for multiple testing and a value below 0.05 for the adjusted p-values were used to determine significant differentially expressed genes. Functional annotation of genes, over representation and gene set enrichment analysis were done using the clusterProfiler package[22]. For visualization of differentially expressed genes and molecular subgroups we used EnhancedVolcano (https://bioconductor.org/packages/EnhancedVolcano/).

Gene-set enrichment GSEA/Single-sample GSEA

GSEA was performed using the most current BROAD javaGSEA standalone version (http://www.broadinstitute.org/gsea/downloads.jsp) and gene signatures of the molecular signature database MsigDB[23,24], 7.4 (Hallmark, C2) as well as published signatures specifying different phenotypic states of melanoma such as gene signatures defining the "transitory-melanocytic" or proliferative state that were taken from Tsoi et al.[25] or Verfaillie et al.[26]. Analyses of single signatures were run using 10,000 permutations; analyses of signature collections were run using 1,000 permutations. Genes were ranked based on the Signal2Noise metric.

Quantitative real-time PCR

RNA isolation from frozen cell pellets was performed with the RNeasy Mini Kit (Qiagen, Germany) and, following the manufacturers protocol. Reverse transcription of 500 ng–2.5 µg RNA was performed with SuperScript VILO cDNA synthesis kit (Invitrogen, Germany) and diluted to a final volume of 50 µl. qRT-PCR was carried out on a Step one plus (Applied Biosystems, Germany) for 30–40 cycles. Primers were designed for 55–60°C annealing temperatures. Relative expression levels were calculated with ΔΔCT, normalized to β-actin. Primer sequences are shown in the Supplementary file, table S2.

Supplementary Materials: The following supporting information can be downloaded at: www.mdpi.com/xxx/s1, Figure S1: Assessment of the label-retaining capacity of reporter cells, Figure S2: Phenotype switching regulates putative mediators of stemness.

Author Contributions: A.V. and T.R. wrote the manuscript and designed the figures. All authors have read and agreed to the published version of the manuscript.

Funding: A.V. and T.R. received funding by the Deutsche Forschungsgemeinschaft DFG (Grant number: 392534127). Open Access Funding by the University of Veterinary Medicine Vienna.

Conflicts of Interest: The authors declare no conflict of interest.

Institutional Review Board Statement: Not applicable.

Informed Consent Statement: Not applicable.

References

1. Rambow, F. et al. Toward Minimal Residual Disease-Directed Therapy in Melanoma. Cell 174, 843-855 e819, doi:10.1016/j.cell.2018.06.025 (2018).
2. Marin-Bejar, O. et al. A neural crest stem cell-like state drives nongenetic resistance to targeted therapy in melanoma. bioRxiv, 2020.2012.2015.422929, doi:10.1101/2020.12.15.422929 (2020).
3. Boiko, A. D. et al. Human melanoma-initiating cells express neural crest nerve growth factor receptor CD271. Nature 466, 133-137, doi:10.1038/nature09161 (2010).
4. Filipp, F. V., Li, C. & Boiko, A. D. CD271 is a molecular switch with divergent roles in melanoma and melanocyte development. Scientific Reports 9, 7696, doi:10.1038/s41598-019-42773-y (2019).
5. Ngo, M. et al. Antibody Therapy Targeting CD47 and CD271 Effectively Suppresses Melanoma Metastasis in Patient-Derived Xenografts. Cell Rep 16, 1701-1716, doi:10.1016/j.celrep.2016.07.004 (2016).
6. García-Silva, S. et al. Melanoma-derived small extracellular vesicles induce lymphangiogenesis and metastasis through an NGFR-dependent mechanism. Nature Cancer, doi:10.1038/s43018-021-00272-y (2021).
7. Lehraiki, A. et al. Increased CD271 expression by the NF-kB pathway promotes melanoma cell survival and drives acquired resistance to BRAF inhibitor vemurafenib. Cell Discov 1, 15030, doi:10.1038/celldisc.2015.30 (2015).
8. Radke, J., Rossner, F. & Redmer, T. CD271 determines migratory properties of melanoma cells. Sci Rep 7, 9834, doi:10.1038/s41598-017-10129-z (2017).
9. Redmer, T. Deciphering mechanisms of brain metastasis in melanoma - the gist of the matter. Mol Cancer 17, 106, doi:10.1186/s12943-018-0854-5 (2018).
10. Redmer, T. et al. The role of the cancer stem cell marker CD271 in DNA damage response and drug resistance of melanoma cells. Oncogenesis 6, e291, doi:10.1038/oncsis.2016.88 (2017).
11. Redmer, T. et al. The nerve growth factor receptor CD271 is crucial to maintain tumorigenicity and stem-like properties of melanoma cells. PLoS One 9, e92596, doi:10.1371/journal.pone.0092596 (2014).
12. Vidal, A. & Redmer, T. Decoding the Role of CD271 in Melanoma. Cancers (Basel) 12, doi:10.3390/cancers12092460 (2020).
13. Holzel, M. & Tuting, T. Inflammation-Induced Plasticity in Melanoma Therapy and Metastasis. Trends Immunol 37, 364-374, doi:10.1016/j.it.2016.03.009 (2016).
14. Kemper, K., de Goeje, P. L., Peeper, D. S. & van Amerongen, R. Phenotype switching: tumor cell plasticity as a resistance mechanism and target for therapy. Cancer Res 74, 5937-5941, doi:10.1158/0008-5472.CAN-14-1174 (2014).
15. Pisco, A. O. & Huang, S. Non-genetic cancer cell plasticity and therapy-induced stemness in tumour relapse: 'What does not kill me strengthens me'. Br J Cancer 112, 1725-1732, doi:10.1038/bjc.2015.146 (2015).
16. Rambow, F., Marine, J. C. & Goding, C. R. Melanoma plasticity and phenotypic diversity: therapeutic barriers and opportunities. Genes Dev 33, 1295-1318, doi:10.1101/gad.329771.119 (2019).
17. Jiang, H., Lei, R., Ding, S. W. & Zhu, S. Skewer: a fast and accurate adapter trimmer for next-generation sequencing paired-end reads. BMC Bioinformatics 15, 182, doi:10.1186/1471-2105-15-182 (2014).
18. Chen, S., Zhou, Y., Chen, Y. & Gu, J. fastp: an ultra-fast all-in-one FASTQ preprocessor. Bioinformatics 34, i884-i890, doi:10.1093/bioinformatics/bty560 (2018).
19. Kim, D. et al. TopHat2: accurate alignment of transcriptomes in the presence of insertions, deletions and gene fusions. Genome Biol 14, R36, doi:10.1186/gb-2013-14-4-r36 (2013).
20. Liao, Y., Smyth, G. K. & Shi, W. The R package Rsubread is easier, faster, cheaper and better for alignment and quantification of RNA sequencing reads. Nucleic Acids Res 47, e47, doi:10.1093/nar/gkz114 (2019).
21. Love, M. I., Huber, W. & Anders, S. Moderated estimation of fold change and dispersion for RNA-seq data with DESeq2. Genome Biol 15, 550, doi:10.1186/s13059-014-0550-8 (2014).
22. Wu, T. et al. clusterProfiler 4.0: A universal enrichment tool for interpreting omics data. Innovation (N Y) 2, 100141, doi:10.1016/j.xinn.2021.100141 (2021).
23. Mootha, V. K. et al. PGC-1alpha-responsive genes involved in oxidative phosphorylation are coordinately downregulated in human diabetes. Nat Genet 34, 267-273, doi:10.1038/ng1180 (2003).
24. Subramanian, A. et al. Gene set enrichment analysis: a knowledge-based approach for interpreting genome-wide expression profiles. Proc Natl Acad Sci U S A 102, 15545-15550, doi:10.1073/pnas.0506580102 (2005).
25. Tsoi, J. et al. Multi-stage Differentiation Defines Melanoma Subtypes with Differential Vulnerability to Drug-Induced Iron-Dependent Oxidative Stress. Cancer Cell 33, 890-904 e895, doi:10.1016/j.ccell.2018.03.017 (2018).
26. Verfaillie, A. et al. Decoding the regulatory landscape of melanoma reveals TEADS as regulators of the invasive cell state. Nat Commun 6, 6683, doi:10.1038/ncomms7683 (2015).
27. Civenni, G. et al. Human CD271-positive melanoma stem cells associated with metastasis establish tumor heterogeneity and long-term growth. Cancer Res 71, 3098-3109, doi:10.1158/0008-5472.CAN-10-3997 (2011).
28. Quintana, E. et al. Phenotypic heterogeneity among tumorigenic melanoma cells from patients that is reversible and not hierarchically organized. Cancer Cell 18, 510-523, doi:10.1016/j.ccr.2010.10.012 (2010).

29. Restivo, G. et al. Publisher Correction: The low affinity neurotrophin receptor CD271 regulates phenotype switching in melanoma. Nat Commun 9, 314, doi:10.1038/s41467-018-02850-8 (2018).

30. D'Aguanno, S., Mallone, F., Marenco, M., Del Bufalo, D. & Moramarco, A. Hypoxia-dependent drivers of melanoma progression. J Exp Clin Cancer Res 40, 159, doi:10.1186/s13046-021-01926-6 (2021).

31. Wagle, N. et al. MAP kinase pathway alterations in BRAF-mutant melanoma patients with acquired resistance to combined RAF/MEK inhibition. Cancer Discov 4, 61-68, doi:10.1158/2159-8290.CD-13-0631 (2014).

32. Fallahi-Sichani, M. et al. Adaptive resistance of melanoma cells to RAF inhibition via reversible induction of a slowly dividing de-differentiated state. Mol Syst Biol 13, 905, doi:10.15252/msb.20166796 (2017).

33. Rambow, F., Marine, J. C. & Goding, C. R. Melanoma plasticity and phenotypic diversity: therapeutic barriers and opportunities. *Genes Dev* **33**, 1295-1318, doi:10.1101/gad.329771.119 (2019).

34. Schatton, T. *et al.* Identification of cells initiating human melanomas. *Nature* **451**, 345-349, doi:10.1038/nature06489 (2008).

35. Gao X, Daugherty RL, Tourtellotte WG. Regulation of low affinity neurotrophin receptor (p75(NTR)) by early growth response (Egr) transcriptional regulators. *Mol Cell Neurosci*. 2007;36(4):501-514. doi:10.1016/j.mcn.2007.08.013

36. Yin, X. *et al.* ATF3, an adaptive-response gene, enhances TGF{beta} signaling and cancer-initiating cell features in breast cancer cells. *J Cell Sci* **123**, 3558-3565, doi:10.1242/jcs.064915 (2010).

37. Leung, C. O. *et al.* Sox9 confers stemness properties in hepatocellular carcinoma through Frizzled-7 mediated Wnt/beta-catenin signaling. *Oncotarget* **7**, 29371-29386, doi:10.18632/oncotarget.8835 (2016).

38. 3   Song, H. *et al.* LncRNA THOR increases the stemness of gastric cancer cells via enhancing SOX9 mRNA stability. *Biomed Pharmacother* **108**, 338-346, doi:10.1016/j.biopha.2018.09.057 (2018).

39. 4   Vand-Rajabpour, F. *et al.* Upregulation of SNAI2 and SOX9 mRNA versus downregulation of eight other EMT/stemness related genes in basal cell carcinoma. *Br J Dermatol* **181**, 1065-1066, doi:10.1111/bjd.17995 (2019).

40. 5   Wu, H. *et al.* LncRNA THOR increases osteosarcoma cell stemness and migration by enhancing SOX9 mRNA stability. *FEBS Open Bio* **9**, 781-790, doi:10.1002/2211-5463.12620 (2019).

41. 6   Zhao, J., Li, H. & Yuan, M. EGR1 promotes stemness and predicts a poor outcome of uterine cervical cancer by inducing SOX9 expression. *Genes Genomics* **43**, 459-470, doi:10.1007/s13258-021-01064-5 (2021).

42. Men, X. *et al.* Overexpression of TMEM47 Induces Tamoxifen Resistance in Human Breast Cancer Cells. *Technol Cancer Res Treat* **20**, 15330338211004916, doi:10.1177/15330338211004916 (2021).

43. Mittal L, Srivastava M, Kumari A, Tonk RK, Awasthi A, Asthana S. Interplay among Structural Stability, Plasticity, and Energetics Determined by Conformational Attuning of Flexible Loops in PD-1. J Chem Inf Model. 2021 Jan 25;61(1):358-384. doi: 10.1021/acs.jcim.0c01080. Epub 2021 Jan 12. PMID: 33433201.